ELSEVIER

Microporous high-surface area layered CeO$_2$

M.C. Cabús-Llauradó, Y. Cesteros, F. Medina, P. Salagre, J.E. Sueiras *

Departament d'Enginyeria Química, Universitat Rovira i Virgili, Països Catalans, 26, Tarragona 43007, Spain

Abstract

A simple procedure for the obtaining of microporous high-surface area layered ceria is described. The synthesis consists of the formation of cerium hydroxide by precipitation of cerium (III) chloride with ammonium carbonate followed by a calcination step. The samples obtained were calcined at temperatures from 150 °C to 350 °C. The effects of calcination temperature on the crystalline phase, particle size, anisotropy, surface area and the textural, morphological and reducibility properties have been studied by powder X-ray diffraction, BET, scanning electron microscopy and temperature-programmed reduction techniques. The anisotropic effects on the particle growth were studied by means of a Williamson–Hall plot.
© 2006 Elsevier Inc. All rights reserved.

Keywords: High-surface area layered cerium dioxide; Microporous

1. Introduction

Cerium (IV) oxide (CeO$_2$, cerianite), with a cubic fluorite-type structure [1] is one of the most reactive rare earth metal oxides. A remarkable property of this material is the number of effective redox Ce^{4+}/Ce^{3+} sites and their ability to exchange oxygen. Therefore, cerianite can be used as a promoter or support in industrial catalytic processes because of its oxygen vacancy defects which can rapidly be formed and removed, causing a remarkable oxygen storage capacity [2,3].

Consequently, ceria has been extensively investigated for catalytic applications, such as three way catalysts in automobile exhaust systems [4–7], in the oxidative dehydrogenation of light alkanes [8,9] or the dehydrogenation of cyclohexanol [10]. Lately, ceria has been used in composite systems [10] or as a support [11,12].

The preparation of CeO$_2$ materials of mesoporous [13,14] and macroporous structured nanoparticles [15] and films [16] has been widely described. Among the methods used to prepare rare earth oxides the thermal decomposition of cerium carbonates or hydroxycarbonates, which allow a morphological, crystal size and physicochemical control of synthesized cerianite [3] and microwave–hydrothermal synthesis [17], can be found. Precipitation of metal salts in alkaline medium followed by a thermal treatment in air has been extensively used for the synthesis of other oxides, such as Fe$_2$O$_3$ [18]. Analogously, cerium oxide has also been prepared by precipitation [19,20]. References concerning the synthesis and structural characterization of microporous CeO$_2$ are not often found in the literature.

In this work, a microporous high surface area cerium oxide has been prepared using an own lab procedure based on a precipitation and a thermal treatment under mild conditions. The effects of calcination temperature on the crystalline phase, particle size, anisotropy, surface area and the textural, morphological and reducibility properties have been studied by XRD, BET, SEM and TPR techniques.

2. Experimental

All chemicals were purchased from Aldrich (Germany), purity $\geqslant$ 99.5%. An aqueous solution of (NH$_4$)$_2$CO$_3$ (0.29 M) was added ($\approx$0.4 mL/min) to a stirring aqueous

* Corresponding author. Fax: +34 977559621.
  E-mail address: jesus.sueiras@urv.cat (J.E. Sueiras).

solution of $CeCl_3 \cdot 7H_2O$ (0.0058 M) until a pH value of 8.5 was reached. The mixture was stirred for 30 min. Then, the solution was decanted, filtered, repeatedly washed till negative chloride test, and calcined at temperatures from 150 to 350 °C for an hour. Part of the material was calcined at 350 °C directly, while the other part was subjected to a slower heating rate.

Powder X-ray diffraction patterns of the samples were collected in a Siemens D5000 diffractometer with Bragg–Brentano geometry using nickel-filtered Cu-Kα radiation ($\lambda = 0.1541$ nm). Data were collected in the 2θ range of 10–70° with an angular step of 0.058 at 3 s per step.

N_2 adsorption and desorption isotherms at 77 K were measured on an automatic Micromeritics ASAP 2020 surface analyzer. Before analysis, the samples were degassed in vacuum at 120 °C for 16 h. The surface area was calculated according to the BET and DFT methods and the micropore size distribution was determined using the Micromeritics DFT software.

Scanning electron microscopy analysis combined with energy dispersive X-ray analysis (SEM–EDX) was carried out in a JEOL JSM6400 scanning microscope operating at an accelerating voltage in the 15–20 kV range. Samples were previously coated with gold by sputtering technique to create contrast.

Temperature programmed reduction (TPR) and oxidation (TPO) measurements were performed using a Thermofinnigan TPDRO 1100 system. A mixture of H_2 (5%) in argon with a flow of 20 mL/min was used to reduce the samples (0.12 g) placed in an oven heated up from 40 °C to 990 °C with a heating rate of 10 °C/min and left at 990 °C for 20 min. The reduction of CuO to metallic copper was used to calibrate the TPR apparatus for H_2 consumption. For the oxidation measurement a mixture of O_2 (5%) in helium was used.

3. Results

3.1. X-ray diffraction measurements (XRD)

XRD measurements of the precipitate were not enough defined due to poor crystallinity of the obtained white and water insoluble precipitate, where cerium oxide carbonate hydrate has probably been obtained.

The XRD analysis of the samples calcined at different temperatures (150–350 °C) and the pattern peaks of reflections corresponding to cubic CeO_2 (JCPDS file 34–394, cerianite, dotted lines) are shown in Fig. 1. The material does not present a crystalline CeO_2 structure neither at 150 °C nor at 200 °C, although the peaks at $2\theta \approx 28.555°$ and at $2\theta \approx 47.479°$ begin to appear. All reflections of the materials calcined at 250 °C to 350 °C are assigned to those typically presented by CeO_2 pattern, in spite of the fact that they all exhibit a shift of 2θ values. The peaks present some diffraction-line broadening. The microstructure analysis was performed by TOPAS version 2.1. using the theory of integral breadth of the diffraction-lines which
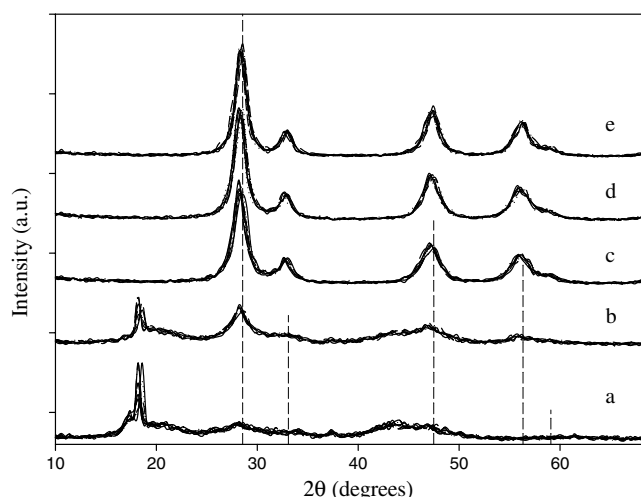

Fig. 1. XRD patterns for CeO_2 calcined at: (a) 150 °C, (b) 200 °C, (c) 250 °C, (d) 300 °C and (e) 350 °C. Dotted lines represent 2θ of cerianite reported data.

assumes an intermediate crystallite size broadening modelled by a Voigt function. In order to evaluate whether the size effect is isotropic or it varies with the lattice direction, a Williamson–Hall plot (inverse of crystallite size, β_f^*, vs. the inverse of plane spacing, d^*) was built (Fig. 2). The lattice parameters for the powders at different temperatures and the crystallite sizes of the catalysts are presented in Table 1. The lattice parameter, a, differs slightly from the theoretical value given for the pattern of CeO_2. As the calcination temperature increases, the value of the lattice parameter, *a*, comes to a better agreement to the reported value. The crystallite size increases with the calcination temperature for all 2θ. The highest 2θ angle ($\approx 59.087°$) has not been considered for the calculations because of the overlapping of the peak and the very high standard deviation, which makes difficult and doubtful the curve fitting calculations [21,22].
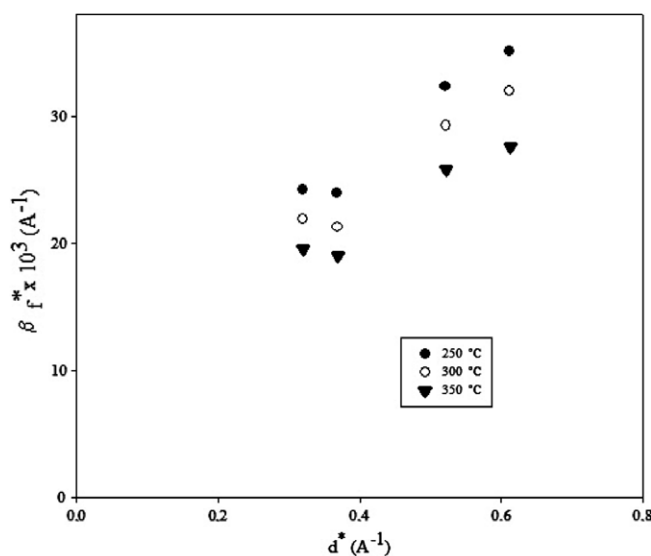

Fig. 2. Williamson–Hall plot for CeO_2 calcined at different temperatures.

Table 1
Influence of calcination temperature on lattice parameter, a, and particle size (values in parentheses refer to the error associated to the calculation)

Pattern (34–394)	$T_{calcination}$ (°C)					
	250		300		350	
$a = 0.54113$ nm	$a = 0.54268$ nm		$a = 0.54270$ nm		$a = 0.54150$ nm	
2θ	2θ	Crystallite size (nm)	2θ	Crystallite size (nm)	2θ	Crystallite size (nm)
28.555	28.4545	4.124 (58)	28.4723	4.561 (57)	28.5515	5.097 (69)
33.082	32.961	4.17 (16)	32.9830	4.69 (17)	33.063	5.24 (19)
47.479	47.31	3.089 (67)	47.3850	3.416 (67)	47.449	3.871 (79)
56.335	56.205	2.848 (87)	56.2100	3.129 (94)	56.323	3.62 (10)
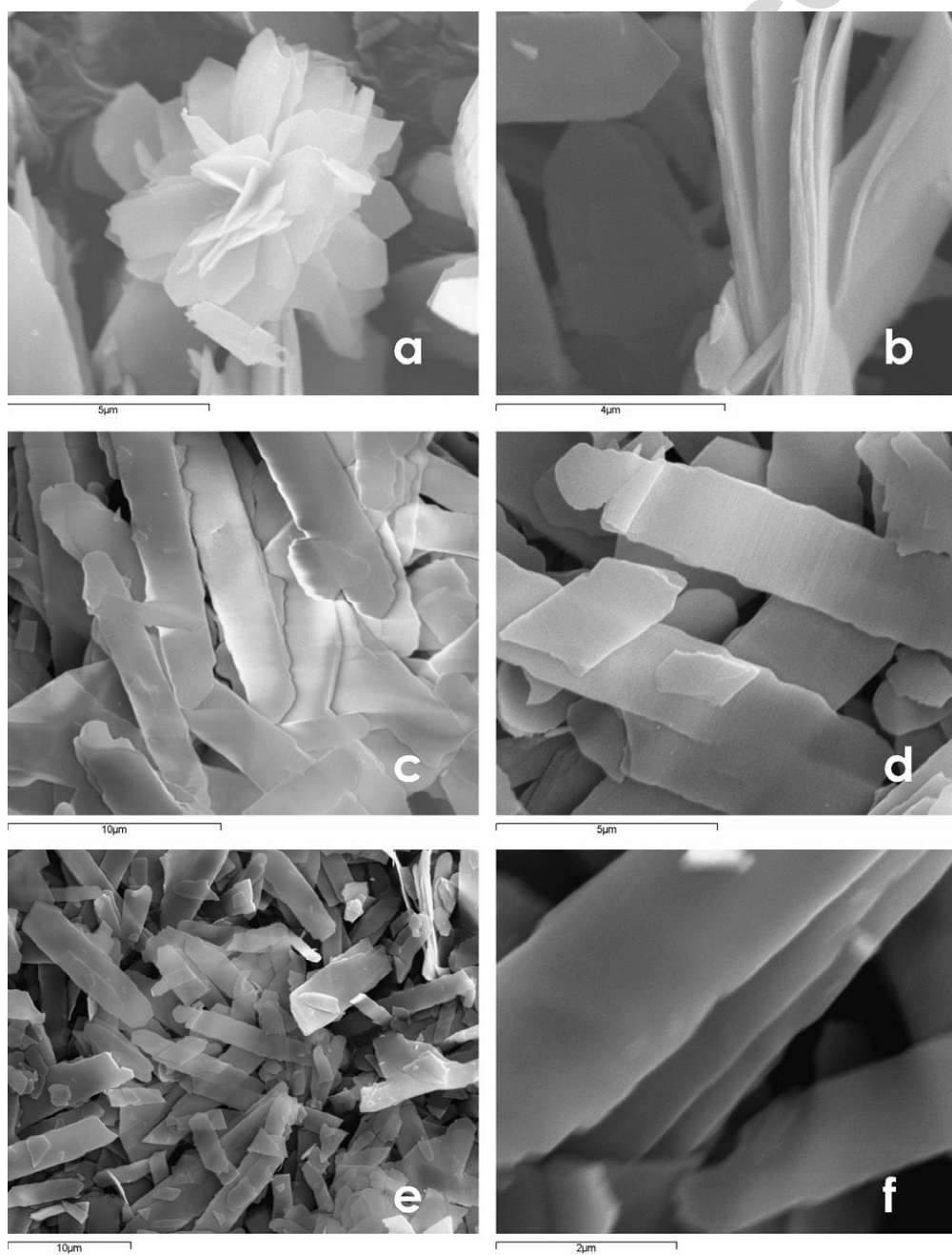
Fig. 3. SEM micrographs of CeO$_2$: (a, b) calcined with a slow heating rate to 350 °C, (c, d) calcined at 350 °C with no heating rate and (d, e) calcined at 300 °C.
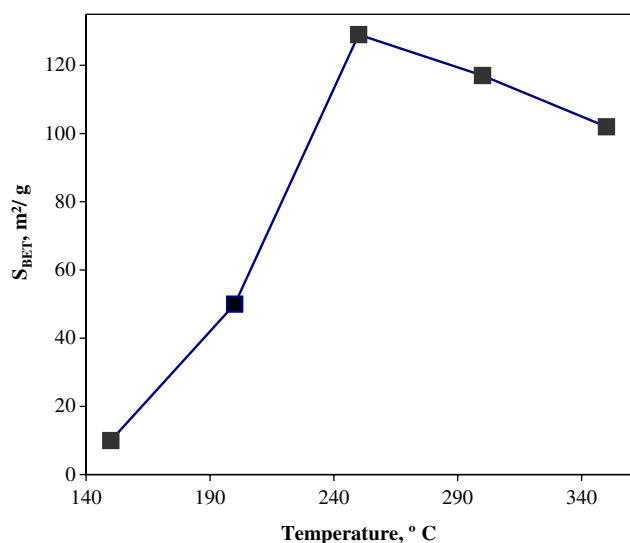
Fig. 4. Effect of calcination temperature on surface area (S_{BET}).

Fig. 6. Micropore size distribution of CeO_2 calcined at 250 °C using the Micromeritics DFT software.

3.2. Scanning electron microscopy (SEM)

The SEM micrographs corresponding to the material calcined at 350 °C (with and without heating rate) and 300 °C (without heating rate) are shown in Fig. 3. In general, the material shows non-uniform size particles. However, the shape of the particles appears to be quite homogeneous consisting in thin long plates (layers of nanometric thickness, around 2 μm wide and variable length higher than 1 μm) with round edges. The material calcined at 350 °C with slower heating rate gave a more ordered structure presenting a rose-like structure (Fig. 3a, b), while
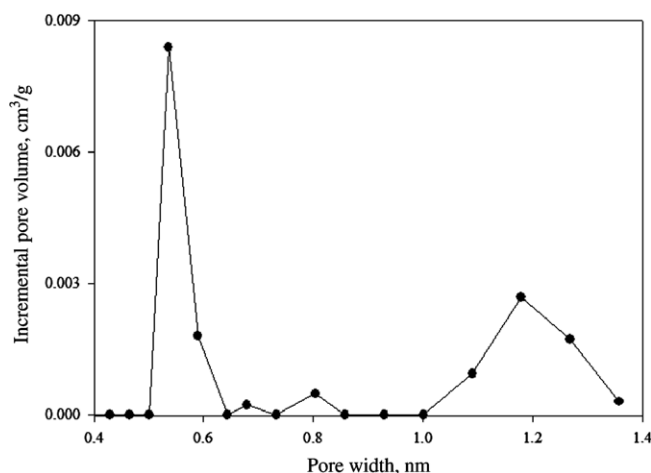
that calcined directly at 350 °C presented separated plates. The layers (petals) forming the rose structure present a quite homogeneous morphology.

3.3. Nitrogen physisorption

The surface area (S_{BET}) was determined by N_2 physisorption technique using the BET method. The effect of the calcination temperature on the surface area is shown in Fig. 4. The S_{BET} suddenly increases at 250 °C; then, it linearly and smoothly decreases when the temperature becomes higher. The adsorption–desorption nitrogen isotherms for CeO_2 prepared at 250 °C and its pore size distribution are shown
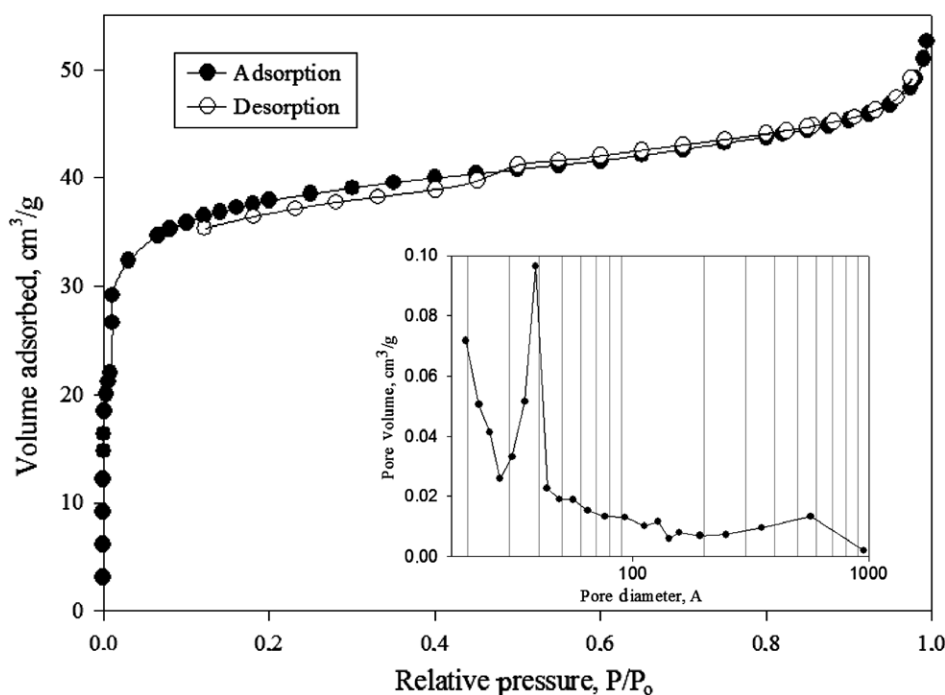

Fig. 5. Adsorption–desorption isotherm for the sample calcined at 250 °C and pore size distribution by BJH method.
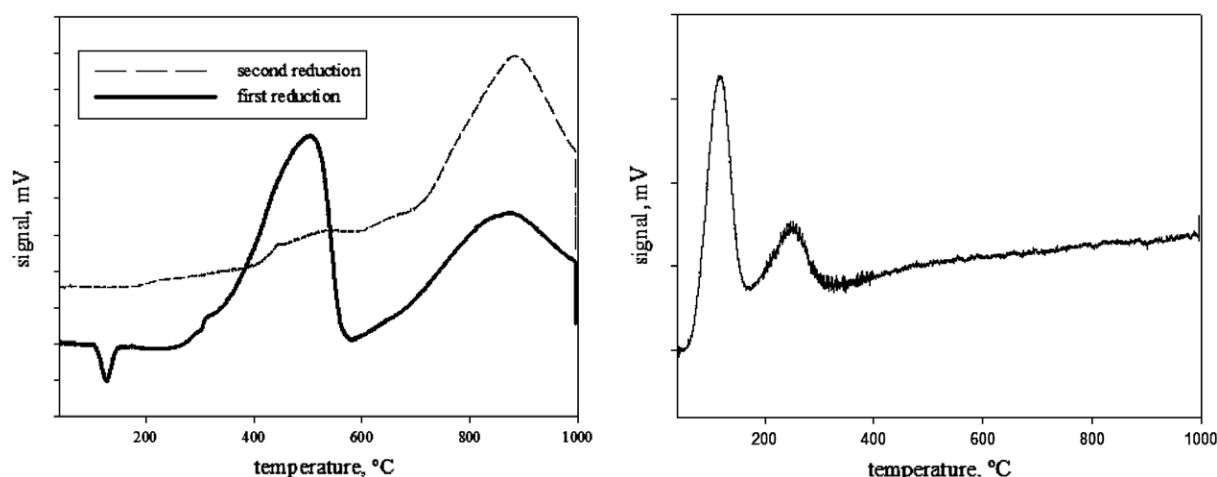
Fig. 7. Redox cycle profile for the CeO$_2$ calcined at 350 °C (reduction: left/oxidation: right).

in Figs. 5 and 6. The material presented a narrow pore width distribution centered at 0.53 nm and a wide region pore size between 1 nm and 1.3 nm. All samples, excepting that prepared at 150 °C, show the same isotherm profile. The microporous areas show a decreasing trend as of 105.0, 96.4 and 82.5 m^2/g for the samples calcined at the increasing 250 °C, 300 °C and 350 °C temperatures, respectively.

3.4. Temperature programmed reduction (TPR) and oxidation (TPO)

The TPR results exhibited a broad reduction profile centred at 502 °C and a high temperature reduction peak at 900 °C (Fig. 7, left) in the first reduction. The quantitative analysis for hydrogen consumption gave the following results: 270 µmol H$_2$/g$_{sample}$ for the first peak and 367 µmol H$_2$/g$_{sample}$ for the peak at the higher temperature. The TPO profile gave a higher peak at 122 °C and a lower one centred at 250 °C. After oxidation, the material was reduced again giving place to a defined peak around 900 °C. From about 400 °C to 700 °C, a non-defined and overlapped peak is detected. Quantitative analysis for hydrogen consumption is difficult due to overlapping. However, a qualitative comparison between the first and second reductions evidenced that the peak at 900 °C entails a higher hydrogen consumption at the second reduction.

4. Discussion

First, concerning the XRD results all reflections of the materials calcined between 250 °C and 350 °C are assigned to those typically shown by the CeO$_2$ pattern.

Considering that the CeO$_2$ has been synthesized by wet soft chemistry, the uniform shape and the 'size' effect are dominant in the line broadening, assuming no strain by microdesorptions in our case. The Williamson–Hall plot gives an overview of the nature of the broadening due to crystal imperfections. The scattering of points is attributed to an anisotropic size effect, which is consistent with the following discussion of SEM analysis. The anisotropic morphology based on thin long plates of CeO$_2$ as shown by SEM, account for the peak broadening of the diffractogram from XRD.

The increase of S_{BET} parallels the increase of CeO$_2$ crystallinity up to 250 °C. Nevertheless, as the calcination temperature increases from 250 to 350 °C, the surface area of CeO$_2$ decreases due to the higher size particles formed and the subsequent loss of microporosity. From the long nearly flat branch with a small 'tail' at higher p/p_0, in the adsorption–desorption isotherm, and the narrow hysteresis loop obtained (Fig. 5) we may classify it as a type I isotherm. The material presents an important microporosity, which is the major responsible for the high surface area of CeO$_2$. The pore size distribution plot (Fig. 6) confirms the presence of microporosity at a predominant pore size of 0,53 nm and also a micropore distribution between 1 nm and 1.3 nm. This microporosity increases from 150 °C to 250 °C. Such increase may be due to the opening of the micropores of lower size carried out by the condensation of vicinal surface-carpeting OH groups to give rise to Ce–O–Ce bridges. This effect is expected to disappear at temperatures above 250 °C.

Regarding the mechanism of reduction of CeO$_2$, it is generally believed to occur via sequential steps: (i) dissociation of chemisorbed hydrogen with formation of OH groups; (ii) formation of anionic vacancies with desorption of water by recombination of H and OH (with concomitant reduction of Ce^{4+} to Ce^{3+}) and (iii) diffusion of surface anionic vacancies into the bulk [23,24]. The TPR profile of CeO$_2$ has been classically interpreted to occur via a stepwise process: first, the relatively fast reduction of the outermost layers of Ce^{4+} (surface reduction) at 502 °C and then, a slower reduction of the inner Ce^{4+} layer (bulk reduction) at 900 °C. This process is controlled by oxygen diffusion in the lattice structure [23]. Nevertheless, more recent studies show that the reduction of CeO$_2$ depends on thermodynamic and kinetic aspects of the small and large crystallites. The reduction of smaller crystallites of CeO$_2$ starts around

240 °C. The limiting factors of achieving a total reduction are not thermodynamic, but kinetic (any of the two first steps in the mechanism of reduction) and the textural changes due to crystallites growth (sintering). The first peak from the first reduction of the TPR profile (Fig. 7, left) results from the balance between both factors. The intensity of the first peak is related to the surface area of the material [25]. As temperature increases, the crystallites grow to give a higher amount of bulk CeO_2, which is responsible for the second peak [25,26]. After the first reduction, the oxidation process was performed to recover the CeO_2 (Fig. 7, right). Since the material had been strongly reduced to very high temperatures, oxidation did not take place at room temperature and had to be heated up [27]. As expected, the second reduction gave place to a defined single-peak (around 900 °C) with a profile indicating very large crystallites of CeO_2 caused by the former reduction and oxidation processes up to 990 °C. However, the overlapped non-defined peak between 400 °C and 700 °C evidences some remaining small crystallites of CeO_2.

5. Conclusions

A simple precipitation method followed by calcination at different temperatures is an effective procedure to obtain a pure crystalline microporous CeO_2 from 250 °C to 350 °C. The growth of CeO_2 particles presents some anisotropy, as shown by XRD, which is consistent with the layered shape of particles observed by SEM.

The morphology of CeO_2 is affected by the heating rate in the thermal process. At 350 °C, a slow heating rate gives place to rose-like layered structure of CeO_2, while fast heating rate calcination yields a layered structure of CeO_2.

The thermal process has an important influence on surface area. At 250 °C, the highest surface area CeO_2 is obtained. At higher temperatures, a decreasing surface area and an increase of particle size are observed. The decrease of microporosity parallels the decrease of surface area and the increase of calcinations temperature between 250 °C and 350 °C.

The high intensity of the first peak in the first reduction process confirms again the high-surface of the obtained material. The exhibited redox reversibility of CeO_2 may be relevant for applications in oxidation–reduction catalysis, processes involving high oxygen-storing capacity, etc.

References

[1] N. Blumental, F.S. Brugner, J.E. Garner, J. Electrochem. Soc. 120 (1973) 1230.
[2] J. Bai, Z. Xu, Y. Zheng, H. Yin, Mater. Lett. 60 (2006) 1287.
[3] C.T. Campbell, C.H.F. Peden, Science 309 (2005) 713.
[4] H. Shinjoh, J. Alloys Compd. 408–412 (2006) 1061.
[5] A. Trovarelli, Catal. Rev. Sci. Eng. 38 (4) (1996) 439.
[6] S. Bernal, J.J. Calvino, M.A. Cauqui, J.M. Gatica, C. Larese, J.A. Perez Omil, J.M. Pintado, Catal. Today 50 (1999) 175.
[7] R. Di Monte, J. Kašpar, Top. Catal. 28 (2004) 47.
[8] R.X. Valenzuela, G. Bueno, A. Solbes, F. Sapiña, E. Martínez, V. Cortés Corberán, Top. Catal. 15 (2001) 2.
[9] R.X. Valenzuela, G. Bueno, V. Cortés Corberán, Y. Xu, C. Chen. Abstracts 215th ACS Nat. Meeting Dallas, 1998, COLL-085.
[10] B. Gopal Mishra, G. Ranga Rao, J. Mol. Catal. A 243 (2006) 20.
[11] P.-Y. Sheng, G.A. Bowmaker, H. Idriss, Appl. Catal. A 261 (2004) 171.
[12] G.B. Hoflund, S.D. Gardner, D.R. Schryer, B.T. Upchurch, E.J. Kielen, React. Kinet. Catal. Lett. 58 (1996) 19.
[13] A. Corma, P. Atienzar, H. Garcia, J.Y. Chane-Ching, Nat. Mater. 3 (2004) 394.
[14] S.C. Laha, R. Ryoo, Chem. Commun. 17 (2003) 2138.
[15] D.S. Bae, B. Lim, B.I. Kim, K.S. Han, Mater. Lett. 56 (2002) 610.
[16] M. Lundberg, B. Skarman, F. Cesar, L.R. Wallenberg, Micropor. Mesopor. Mater. 54 (2002) 97.
[17] A. Bonamartini Corradi, F. Bondioli, A.M. Ferrari, T. Manfredini, Mater. Res. Bull. 41 (2006) 38.
[18] M.P. Morales, S. Veintemillas-Verdaguer, M.I. Montero, C.J. Serna, Chem. Mater. 11 (1999) 3058.
[19] T.J. Kirk, J. Winnick, J. Electrochem. Soc. 140 (1993) 3494.
[20] T. Kirk, J. Winnick, in: Proceedings of the 27th Inter-society Energy Conversion Engineering Conference, August 1992.
[21] R.L. Snyder, J. Fiala, H.J. Bunge, Defect and microstructure analysis by diffraction, in: International Union of Crystallography, Monographs on Crystallography, vol. 10, Oxford Science Publications, 1999.
[22] TOPAS 3.1, General profile and structure analysis software for powder diffraction data, User's manual, Bruker AXS GmbH, Karlsruhe, Germany.
[23] J.E. Fallah, S. Boujana, H. Dexpert, A. Kiennemann, J. Majerus, O. Touret, F. Villain, F. Le Normand, J. Phys. Chem. 98 (1994) 5522.
[24] S. Bernal, J.J. Calvino, G.A. Cifredo, J.M. Rodríguez-Izquierdo, J. Phys. Chem. 99 (1995) 11794.
[25] F. Giordano, A. Trovarelli, C. de Leitenburg, M. Giona, J. Catal. 193 (2000) 273.
[26] E. Aneggi, M. Boaro, C. Leitenburg, G. Dolcetti, A. Trovarelli, J. Alloys Compd. 408–412 (2006) 1096.
[27] S. Bernal, G. Blanco, M.A. Cauqui, G.A. Cifredo, J.M. Pintado, J.M. Rodríguez-Izquierdo, Catal. Lett. 53 (1998) 51.